Specification of surface figure and finish in terms of system performance

E. L. Church and P. Z. Takacs

We describe methods of predicting the degradation of the performance of a simple imaging system in terms of the statistics of the shape errors of the focusing element and, conversely, of specifying those statistics in terms of requirements on image quality. Results are illustrated for normal-incidence, x-ray mirrors with figure errors plus conventional and/or fractal finish errors. It is emphasized that the imaging properties of a surface with fractal errors are well behaved even though fractal-power spectra diverge at low spatial frequencies.

Key words: X-ray imaging, surface scattering, surface finish, surface figure, fractal surfaces, surface specification.

1. Introduction

Brookhaven National Laboratory is the site of the National Synchrotron Light Source, an electron synchrotron that is an intense source of hard and soft x rays. Since there are no effective refracting elements for x rays, this radiation must be manipulated and focused by mirrors configured to give high reflectivity.

In the case of hard x rays this is done with high-Z metal mirrors illuminated at glancing angles of incidence below the critical angle for total external reflection. Most synchrotron mirrors and high-energy x-ray telescopes use this method. In the case of soft x rays, reasonable normal-incidence reflectivity can be achieved with multilayer interference coatings.

There are two further differences between x-ray and conventional optics resulting from the short radiation wavelengths involved: The image quality is more sensitive to shape errors in the optical elements, and, even in the case of a perfectly shaped mirror, the image is generally system rather than diffraction limited.

Several years ago we developed a simple diffraction theory for the imaging of glancing-incidence x-ray mirrors that we called the five-factor formula; it related the image quality of system-limited optics to the statistics of the errors in the mirror shape.[1] In this paper we describe the generalization of those results to normal-incidence optics.[2,3]

Although we discuss this method with reference to shape errors in x-ray mirrors, the formalism is also applicable to other sources of wave-front errors, to arbitrary radiation wavelengths, and to refractive optics.

2. Diffraction Theory of Imaging

To display the physics involved most clearly, we consider the paraxial imaging of an on-axis parabolic mirror with statistically symmetric shape errors. The object is to develop simple relationships between shape errors and image quality and, conversely, to specify limits on the statistics of those errors in terms of performance requirements.

The diffraction expression for the measured angular distribution of the reflected and scattered intensity in the image plane is given by

$$I(\boldsymbol{\theta}) = \frac{1}{I_i R}\frac{\mathrm{d}I}{\mathrm{d}\boldsymbol{\theta}} = \frac{1}{\lambda^2}\int \mathrm{d}\boldsymbol{\tau}\,\exp(i2\pi\mathbf{f}\cdot\boldsymbol{\tau})\mathrm{OTF}(\boldsymbol{\tau}), \quad (1)$$

where

$I(\boldsymbol{\theta})$ is the measured intensity distribution or spread function in the image plane as a function of the deflection angles $\boldsymbol{\theta}$, including both system effects and surface-shape errors. It is normalized so that integration over all angles gives unity.

$I_s(\boldsymbol{\theta})$ is the corresponding expression for the system spread function, i.e., the image-intensity distribution for zero surface errors.

E. L. Church is with USA ARDEC, Picatinny Arsenal, New Jersey 07806-5000. P. Z. Takacs is with the Brookhaven National Laboratory, Upton, New York 11973-5000.

Received 11 November 1992.
0003-6935/93/3344-10$06.00/0.

I_i is the total incident intensity.

R is the normal-incidence intensity-reflection coefficient.

$d\theta$ is the solid angle element.

λ is the radiation wavelength.

τ is the lag vector in the surface plane, which is related to the spatial-frequency vector in the image plane $\mathbf{g}$, through $\mathbf{g} = \tau/\lambda F$, where F is the focal distance.

$\mathbf{f}$ is the spatial frequency in the mirror plane, which is related to the image directions θ and φ by the normal-incidence form of the vector grating equation:

$$\mathbf{f} = \begin{pmatrix} f_x \\ f_y \end{pmatrix} = \frac{\sin\theta}{\lambda}\begin{pmatrix} \cos\varphi \\ \sin\varphi \end{pmatrix} \approx \frac{\boldsymbol{\theta}}{\lambda}. \tag{2}$$

OTF (τ) is the total optical transfer function of the system, normalized to unity at zero lag.

The total OTF is the product of two factors:

$$\mathrm{OTF}(\tau) = \mathrm{OTF}_s(\tau) \times \mathrm{OTF}_e(\tau). \tag{3}$$

The first accounts for system effects and the second for the surface errors. For a perfectly shaped surface, $\mathrm{OTF}_e(\tau) = 1$, and Eq. (1) gives the system spread function $I_s(\theta)$. The system and error OTF factors are discussed in detail in the next two sections.

3. System OTF

The system factor in the total OTF can be written as the product of three subfactors:

$$\mathrm{OTF}_s(\tau) = A_1(\tau) \times A_2(\tau) \times A_3(\tau), \tag{4}$$

which account for illumination, source, and detector effects, as described below.

A. Illumination Factor

A_1 is the illumination factor, which is the autocorrelation of the pupil function. For a simple circular pupil of diameter D_0

$$A_1(\tau) = \frac{2}{\pi}\left\{\arccos\left(\frac{\tau}{D_0}\right) - \frac{\tau}{D_0}\left[1 - \left(\frac{\tau}{D_0}\right)^2\right]^{1/2}\right\}, \tag{5}$$

which, taken alone, leads to the well-known Airy distribution for the image intensity:

$$I_1(\theta) = \frac{\pi}{4}\left(\frac{D_0}{\lambda}\right)^2\left[\frac{J_1(\pi D_0\theta/\lambda)}{\pi D_0\theta/2\lambda}\right]^2. \tag{6}$$

B. Source-Size Factor

A_2 is the source-size factor. In the case of x rays the source is modeled as a collection of incoherent point sources with a Gaussian angular distribution with the rms angular width θ_s. The source-size factor is then

$$A_2(\tau) = \exp[-(\pi\theta_S\tau/\lambda)^2], \tag{7}$$

which corresponds to the intensity distribution

$$I_2(\theta) = \frac{1}{\pi{\theta_S}^2}\exp[-(\theta/\theta_s)^2]. \tag{8}$$

C. Detector-Size Factor

A_3 is the detector-size factor. In the case of a cylindrical detector response with an angular diameter θ_D, it has the sombrero-function form

$$A_3(\tau) = \frac{J_1(\pi\theta_D\tau/\lambda)}{\pi\theta_D\tau/2\lambda}, \tag{9}$$

and the corresponding measured intensity distribution is

$$I_3(\theta) = \frac{4}{\pi{\theta_D}^2}\,\mathrm{Cyl}(\theta/\theta_D), \tag{10}$$

where $\mathrm{Cyl}(x) = 1$ for $|x| < 1/2$ and zero otherwise.

D. Form of the System Spread Function

The fact that Eq. (4) is in the form of a product means that the system spread function is the triple convolution of the intensity distributions given in Eqs. (6), (8), and (10):

$$I_s(\theta) = I_1(\theta) * I_2(\theta) * I_3(\theta). \tag{11}$$

Each term and its convolution have a unit volume, corresponding to the fact that each A and their product are unity at zero lag. These unit properties are statements of the conservation of energy.

The analytic form of the system spread function derived in this way is complicated. In this paper, however, we are less interested in the form of that function than in how it is modified by the presence of surface errors. For that purpose we choose a simple Gaussian form for the system OTF:

$$\mathrm{OTF}_s(\tau) = \exp[-(\pi\tau/W)^2], \tag{12}$$

where W is a length parameter characterizing the width of the system OTF, which we call the coherence length on the surface of the optic.

The corresponding form for the system spread function is

$$I_s(\theta) = \frac{1}{\pi}\left(\frac{W}{\lambda}\right)^2\exp[-(W\theta/\lambda)^2], \tag{13}$$

which has the rms width:

$$\text{width } I_s(\theta) = \frac{\lambda}{W} \triangleq \theta_0. \tag{14}$$

E. System-Limited Optics

The relative importance of the three terms in Eq. (11) depends on the radiation wavelength; the width of the illumination term I_1 is proportional to λ, while I_2 and I_3 are independent of λ. This means that the illumination term dominates at long wavelengths, while the

others dominate at short wavelengths. In other words, visible-light optics may be diffraction limited, but x-ray optics tend to be system limited.[3]

For example, a 10-cm-diameter mirror imaging 140-Å (14-nm) radiation has a diffraction width of the order of a tenth of a microradian, compared with typical source–detector widths of tens or hundreds of microradians.

Equation (14) shows this in a different way. In the diffraction-limited case the coherence length W is a constant equal to the diameter of the focusing element, and the image width is proportional to λ. In the system-limited case, on the other hand, the image width is a constant, and it is the coherence length, which is now smaller than the diameter of the mirror, that is proportional to λ.

If the system described above has a combined source–detector diameter of 100 μrad (21 arcsec), W is only 0.140 mm. Halving λ halves W.

4. Error OTF

A. Relationship to the Surface-Structure Function

The second factor in the total OTF, OTF_e, accounts for the effects of the phase modulation introduced into the reflected wave front by the shape errors in the mirror surface. If those errors are members of Gaussian random processes,

$$\mathrm{OTF}_e(\boldsymbol{\tau}) = \exp\left[-\frac{1}{2}\left(\frac{4\pi}{\lambda}\right)^2 D(\boldsymbol{\tau})\right], \tag{15}$$

where $D(\boldsymbol{\tau})$ is the structure function of the shape errors $Z(\mathbf{x})$,[4]

$$D(\boldsymbol{\tau}) = \langle[Z(\mathbf{x}+\boldsymbol{\tau}) - Z(\mathbf{x})]^2\rangle. \tag{16}$$

Here $\mathbf{x}$ is the position vector in the mirror plane, and $\boldsymbol{\tau}$, the lag, is the vector distance between two such surface points. In other words, the structure function is the mean-square value of the difference in height errors as a function of their separation. If the surface errors are statistically isotropic, as taken in this paper, $D(\boldsymbol{\tau})$ depends only on the magnitude of $\boldsymbol{\tau}$ and not its direction.

In the case of a transmitting rather than a reflective optics, Eq. (16) is multiplied by $[(N-1)/2]^2M$, where N is its index of refraction and M is the number of interfaces involved.

B. Relation to the Power Spectral Density

The structure function appears naturally in the expression for the error OTF and carries the information about the shape errors that determines their effects on the image-intensity distribution.[5]

Valuable insight, however, can be gained by expressing these effects in terms of a mathematically equivalent statistic, the two-dimensional power spectral density of the errors $S_2(\mathbf{f}')$, which describes how the errors are distributed among different spatial frequencies $\mathbf{f}'$. In the case of isotropically rough surfaces the spectrum depends on the magnitude of $\mathbf{f}'$ and not its direction, and we can express the results in terms of the even more accessible function, the one-dimensional or profile power spectrum $S_1(f_x')$.[6]

The description in terms of the two-dimensional spectrum has been discussed in earlier publication.[2,3] In this paper we use the one-dimensional form since it is the quantity that is most directly measured (estimated) from profile measurements of the surface-height errors $Z(x)$.

The profile or one-dimensional power spectrum is defined as

$$S_1(f_x') = \lim_{L\to\infty}\left\langle\frac{2}{L}\left|\int_{-L/2}^{+L/2} \mathrm{d}x\,\exp(i2\pi f_x' x)Z(x)\right|^2\right\rangle, \tag{17}$$

where f_x' is the spatial frequency, i.e., the reciprocal of the spatial wavelength. The structure function is related to this by the integral transform

$$D(\tau) = 4\int_0^\infty \mathrm{d}f_x' S_1(f_x')\sin^2(\pi f_x'\tau). \tag{18}$$

In fact, Eqs. (17) and (18) show the preferred way of determining (estimating) the structure function from measured profile data $Z(x)$, since it allows the bandwidth and transfer-function effects that are present in all real measurements to be accounted for in a direct way.[7,8]

5. Error Models

A. Figure Errors

Surface topographic errors are generally viewed as the sum of two independent components, figure and finish. Figure errors are those left by the shaping process in manufacture and generally have spatial wavelengths from D_0 down to, say, $D_0/10$, where D_0 is the diameter of the mirror. They are usually measured by interferometry and expressed in terms of Zernike polynomials.

If, as is usually the case, the dominant components of the figure spectrum have wavelengths that are much longer than the coherence length W, their contribution to the total structure function is

$$D(\tau) = \tfrac{1}{2}\mu_0^2\tau^2, \tag{19}$$

where μ_0 is the rms gradient of the figure errors. This quantity is related to the figure component of the profile spectrum by

$$\mu_0^2 = 2\int_0^\infty \mathrm{d}f_x' S_1(f_x')(2\pi f_x')^2, \tag{20}$$

where the factor of 2 accounts for the fact that the mean-square surface gradient is twice the mean-square profile slope for an isotropically rough surface.[9]

B. Finish Errors

Finish errors are errors left by the finishing or polishing process and cover the entire spatial-

wavelength spectrum from near-atomic dimensions to the mirror diameter. They are usually measured by one- or two-dimensional profilometry and are characterized in terms of their one- or two-dimensional power spectral densities.

The general form of the finish structure function is sketched in Fig. 1. It vanishes at zero lag, behaves as a power law for low lags, and, after a distance characterized by the correlation length l_0, reaches a saturation value of $2\sigma_0^2$, where σ_0 is the rms roughness of the finish component of the surface errors.

We can distinguish two extreme types of finish error, conventional and fractal, depending on whether the correlation length is much smaller or much larger than other characteristic lengths in the system.[7–10] These are described next.

C. Conventional Surface Finish

One model for conventional surfaces that appears frequently in the earlier literature is that corresponding to an exponential correlation function. Its structure function has the form

$$D(\tau) = 2\sigma_0^2[1 - \exp(-\tau/l_0)], \tag{21}$$

which corresponds to the profile spectrum[6]

$$S_1(f_x') = 4\sigma_0^2 l_0[1 + (2\pi l_0 f_x')^2]^{-1}. \tag{22}$$

Equations (21) and (22) [and Eq. (36)] are special cases of the more general *ABC* or *K*-correlation model.[8]

Note that conventional surfaces are characterized by two intrinsic length parameters: correlation lengths and rms roughnesses.

D. Fractal Surface Finish

Fractal surfaces, on the other hand, have structure functions of the form

$$D(\tau) = T^2(\tau/T)^{n-1}, \tag{23}$$

which is characterized by two different intrinsic finish parameters: the number n called the spectral index and the length parameter T called the topothesy.[10] The topothesy is the average lag distance between two surface points whose connecting chord has an rms slope of unity, and it is usually expressed in angstroms. The larger T, the rougher the surface.

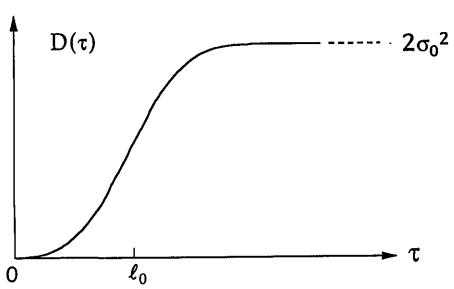

Fig. 1. General form of the structure function of a randomly rough surface.

For a strict mathematical fractal (i.e., $l_0 \to \infty$) the spectral index n must lie between 1 and 3 and is related to the fractal dimension by

$$\text{Hausdorff–Besicovitch dimension of surface} = (7 - n)/2, \tag{24}$$

which is greater than its Euclidian dimension of 2.

The profile power spectrum corresponding to Eq. (23) is

$$S_1(f_x') = K/f_x'^n, \tag{25}$$

where

$$K = -\pi^{(1/2)-n}\frac{\Gamma\left(\frac{n}{2}\right)}{\Gamma\left(\frac{1-n}{2}\right)}T^{3-n}. \tag{26}$$

In practice the finish parameters n and K are determined most simply and accurately by measuring surface profiles, estimating the profile spectrum, and plotting the results on log–log scales.[7] In that case a fractal spectrum appears as a straight line with a negative slope, from which n and K can be determined in a straightforward way.[8]

E. Illustration

Figure 2 shows a typical plot of this type for an x-ray synchrotron mirror measured at Brookhaven. The fractal character of its finish error is shown by the underlying linear structure, and the figure errors appear as additive bumps at low frequencies. Note that the figure errors lie well below the spatial frequency $1/\sqrt{2}W = 5.05 \times 10^{-3}$ μm^{-1} for the example considered above.

Most of the high-performance surfaces we have examined appear to be composed of one or more fractallike finish components with $(n, T) \approx (1.5, 1.5$

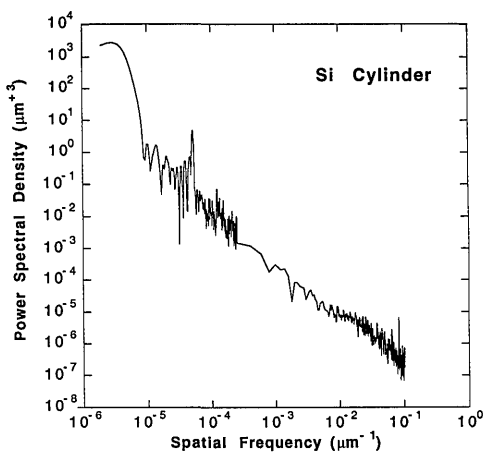

Fig. 2. Profile-power spectral density of a silicon x-ray synchrotron-radiation mirror plotted on log–log scales. Two types of measuring instrument were used to cover the range of spatial frequencies shown.

Å) plus long-wavelength figure errors. The surface in Fig. 2, for example, has been modeled as $n = 4/3$, $K = 3 \times 10^{-8}$ $\mu m^{5/3}$ (i.e., $T = 1.43$ Å) plus figure errors with a total rms slope of the order of 2 μrad (i.e., an rms gradient of 4 μrad).[1]

6. Image Effects for Arbitrary Roughness

Results to this point can be summarized in the following expression for the image-intensity distribution:

$$I(\boldsymbol{\theta}) = \frac{1}{\lambda^2}\int d\boldsymbol{\tau} \exp(i2\pi \mathbf{f}\cdot\boldsymbol{\tau})\exp[-(\pi\tau/W)^2] \times \exp[-(2\pi\mu_0\tau/\lambda)^2]\exp[-(4\pi/\lambda)^2 D(\boldsymbol{\tau})/2]. \quad (27)$$

The first factor in the integrand is the diffraction kernel, the second is the system OTF, and the third and fourth account for the figure and finish errors discussed in Section 5.

This represents the direct solution of the imaging problem. That is, it gives the image-intensity distribution in terms of the figure and finish errors. It must be evaluated numerically for rough surfaces, although several general properties are described below.

A. Figure Effects 1

The exponents of the system and figure factors in Eq. (27) are both proportional to τ^2 and can be combined into a single term with the same form as the system OTF discussed above, except that the coherence length W appearing there is replaced by

$$W' = W\left[1 + 4\left(\frac{W}{\lambda}\right)^2 {\mu_0}^2\right]^{-1/2}. \quad (28)$$

This means that figure errors lower and broaden the Gaussian form of the system spread function. In particular, the on-axis peak height is lowered by the factor

$$\frac{I(0)}{I_s(0)} = \left(\frac{W'}{W}\right)^2, \quad (29)$$

and its rms width is increased by the factor

$$\frac{\text{width } I(\boldsymbol{\theta})}{\text{width } I_s(\boldsymbol{\theta})} = \left(\frac{W'}{W}\right)^{-1}. \quad (30)$$

The algebraic simplicity of these results depends on the fact that we have taken the system spread function to be Gaussian [Eq. (13)].

B. Figure Effects 2

Figure errors appear in one of the factors in the integrand of Eq. (27). But since that integral is in the form of a Fourier transform, their effects can be rewritten as the convolution

$$I(\boldsymbol{\theta}) = \frac{1}{4\pi{\mu_0}^2}\exp[-(\theta/2\mu_0)^2] * I'(\boldsymbol{\theta}), \quad (31)$$

where the first factor on the right is the distribution function of the gradient of the figure errors and the second is the finish-aberrated image intensity. In this case the distribution function is Gaussian since the figure errors were taken to have a Gaussian distribution,[4] and the factor of 2 in the exponent accounts for the doubling of the deflection angle on reflection.

This convolutional way of accounting for finish effects is more general than that in Subsection 6.B since it is not limited to Gaussian forms for the system and distribution functions.

C. Finish Effects

In the case of conventional surfaces, where the intrinsic correlation length is much smaller than the coherence length, the intensity distribution in and about the image can be written as

$$I(\boldsymbol{\theta}) = \exp[-(4\pi\sigma_0/\lambda)^2] \times I''(\boldsymbol{\theta}) + c, \quad (32)$$

where $I''(\boldsymbol{\theta})$ is the figure-aberrated image intensity and c is a small quantity representing the scattered intensity. The exponential factor is the well-known Strehl or Debye–Waller factor, which reduces the specular core without changing its shape.[4]

Despite its wide use in the literature, it should be noted that this simple factor does not necessarily hold for rough surfaces with non-Gaussian height distributions, for long correlation lengths or for fractal surfaces. In those cases Eq. (27) must be examined in detail.

7. Image Effects in the Smooth-Surface Limit

To gain deeper insight into the effects of errors on the image, we consider the smooth-surface limit. That is, we linearize the dependence of the image on the surface errors by replacing the exponential figure and finish factors in Eq. (27) by the first two terms in their power-series expansions. This is a reasonable limit to consider, since we are interested in specifying error in terms of deviations from the ideal imaging behavior, and that requires knowledge of the indicial dependence of the image on the errors.

Strictly speaking, we do not have to take the smooth-surface limit for figure errors since an arbitrary amount of the figure can be taken into account by the methods described above. Here, however, we treat figure and finish on an equal footing by taking the smooth-surface limit of both.

A. Image Distribution for Figure Plus Conventional Finish

In the case of conventional surfaces the image-intensity distribution is given by

$$I(\boldsymbol{\theta}) = I_s(\boldsymbol{\theta})\left\{1 - \frac{4}{{\theta_0}^2}{\mu_0}^2\left[1 - \left(\frac{\theta}{\theta_0}\right)^2\right] - \left(4\pi\frac{\sigma_0}{\lambda}\right)^2\right\} + \frac{16\pi^2}{\lambda^4}\bar{S}_2(\mathbf{f}). \quad (33)$$

The first term on the right is the specular core, the

second is the scattering term, which is proportional to the two-dimensional or area power spectral density of the surface finish.[11] This in turn is related to the finish structure function by

$$S_2(\mathbf{f}) = \int d\boldsymbol{\tau} \exp(i2\pi\mathbf{f}\cdot\boldsymbol{\tau})C(\boldsymbol{\tau}), \tag{34}$$

where

$$C(\boldsymbol{\tau}) = \sigma_0^2 - \tfrac{1}{2}D(\boldsymbol{\tau}) \tag{35}$$

is the autocovariance function of the finish height fluctuations.[12]

For example, in the case of isotropic surfaces with an exponential covariance function considered above,

$$S_2(\mathbf{f}) = 2\pi\sigma_0^2 l_0^2[1 + (2\pi l_0 f)^2]^{-3/2}. \tag{36}$$

This differs from the corresponding one-dimensional form in Eq. (22), since Eq. (22) involves the cosine transform of the correlation function, while Eq. (36) involves its Bessel transform.[6] Again, these examples are special cases of the more general *ABC* model that we have found useful for parameterizing data.[8]

B. Image Distribution for Figure Plus Fractal Finish

In the case of fractal surfaces the image-intensity distribution is given by

$$I(\boldsymbol{\theta}) = I_s(\boldsymbol{\theta})\left\{1 - \frac{4}{\theta_0^2}\mu_0^2\left[1 - \left(\frac{\theta}{\theta_0}\right)^2\right]\right\} + \frac{16\pi^2}{\lambda^4}\left[\frac{\Gamma\left(\frac{1+n}{2}\right)\Gamma\left(\frac{1-n}{2}\right)}{2\sqrt{\pi}\Gamma(n/2)}K\right]W^{n+1} \times {}_1F_1\left[\frac{1+n}{2}; 1; -\left(\frac{\theta}{\theta_0}\right)^2\right], \tag{37}$$

where ${}_1F_1$ is a confluent hypergeometric function. Again, the results are in the form of the sum of the two terms, which are similar to the specular and scattering terms that appear for conventional surfaces.

Here, however, the scattering term is not a small additive constant near the optic axis but is larger and has a strong angular dependence that modifies the shape of the total image, so that the image care is no longer a scaled version of the system spread function. In other words, the Strehl ratio $I(\theta)/I_s(\theta)$ is no longer independent of θ.

C. Large-Angle Scattering

At large angles, far from the image core, only the scattering terms in Eqs. (33) and (37) survive and appear in the common form

$$I(\boldsymbol{\theta}) \to \frac{16\pi^2}{\lambda^4}S_2(\mathbf{f}), \tag{38}$$

where S_2 is again the two-dimensional power spectral density of the surface finish and $\mathbf{f} = \boldsymbol{\theta}/\lambda$.[11]

Equation (36) gives the two-dimensional spectrum for conventional surfaces with an exponential correlation function, while the corresponding form for fractal surfaces is[8–10]

$$S_2(\mathbf{f}) = \frac{\Gamma\left(\frac{1+n}{2}\right)}{2\sqrt{\pi}\Gamma(n/2)} \times \frac{K}{f^{n+1}}, \tag{39}$$

where n and K are the same parameters as in the profile spectrum [Eq. (25)].

D. Illustrations

Figure 3 shows the image-intensity distribution for a surface with conventional finish errors, calculated from Eqs. (33) and (36) for an rms roughness of $\sigma_0 = 5$ Å and a correlation length $l_0 = 1$ μm. The system parameters are a radiation wavelength of 140 Å and a combined source–detector width of $\theta_0 = 100$ μrad.

The shape of the image core is seen to be unchanged by the presence of the finish errors, except for the overall reduction of its intensity, by 20.1% in this example. The scattering term appears as the broad low-intensity background.

In Fig. 4 we show the corresponding results for a surface with fractal finish errors, calculated from Eqs. (37) and (39) for $n = 4/3$ and $K = 1 \times 10^{-8}$ μm$^{5/3}$; i.e., $T = 0.738$ Å. These are the same parameters as those for the surface in Fig. 1, except that K has been reduced by a factor of 3 to satisfy the smooth-surface condition. In this case the on-axis intensity is reduced by 17.2%.

Note that, even though the fractal power spectrum diverges in the low-frequency (small-angle) limit, imaging theory gives the finite results shown since the low-frequency components that diffract into the image core are automatically damped out. The strong low-frequency components that diffract outside the core, however, are unaffected and lead to the broadening of the image shown in the figure.

8. Nonparametric Solution

Equations (33) and (37) are parametric solutions of the inverse problem; that is, they express the image-

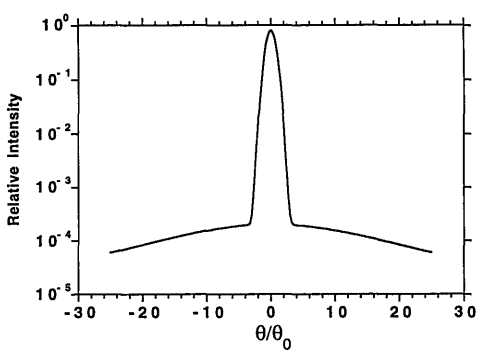

Fig. 3. Image-intensity distribution for a conventional surface calculated from Eq. (33) for $\theta_0 = \lambda/W = 100$ μrad, $\lambda = 140$ Å; $\mu_0 = 0$, $\sigma_0 = 5$ Å, and $l_0 = 1$ μm. In this case the Strehl factor multiplying the image core is 0.799.

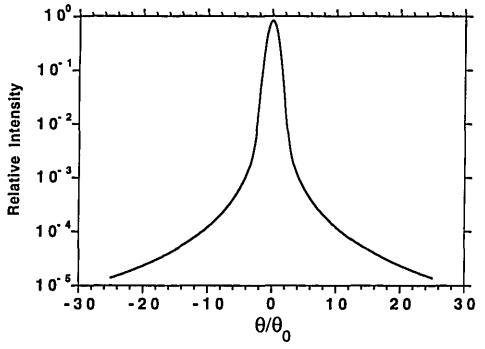

Fig. 4. Image-intensity distribution for a fractal surface calculated from Eq. (37) for the same system and figure parameters as in Fig. 3, but $n = 4/3$ and $K = 1 \times 10^{-8}$ $\mu m^{5/3}$. In this case the on-axis Strehl factor is 0.828.

intensity distribution in terms of figure and finish parameters of the surface errors that can be measured in the laboratory. They have the advantage of giving the entire image-intensity distribution but the disadvantage of being model specific.

In this section we use the smooth-surface approximation to develop nonparametric or model-independent connections between image properties and the profile statistics. We do this by expanding the image intensity in a power series in the angle observation angle θ and expressing the results in terms of the profile power spectrum by using Eq. (18). The first term in this expansion determines the on-axis Strehl factor, and the next nonvanishing term, which is quadratic in θ, gives a measure of the image broadening.

A. Effects on the On-Axis Image Intensity

The on-axis Strehl ratio is easily seen to be

$$\frac{I(0)}{I_s(0)} = 1 - \left(\frac{4\pi}{\lambda}\right)^2 \int_0^\infty df_x' S_1(f_x') K_0(f_x'), \qquad (40)$$

where the kernel in the integral over the error spectrum is

$$K_0(f_x') = 1 - {}_1F_1[1; \tfrac{1}{2}; -(Wf_x')^2]. \qquad (41)$$

This is an important factor since it determines how the different frequency components in the surface profile f_x' affect the on-axis intensity.

The form of this kernel is shown in Fig. 5. The fact that it vanishes at low frequencies means that the effects of long-wavelength components of the figure and finish errors are attenuated, while those with wavelengths longer than the coherence length W enter with full strength.

Equation (40) is valid for any form of the surface spectrum. In the case of conventional surfaces the major part of the spectral integral comes from high frequencies where $K_0 = 1$, the integral becomes the mean-square surface roughness σ_0^2, and we obtain the smooth-surface form of the conventional Strehl factor appearing in Eq. (32).

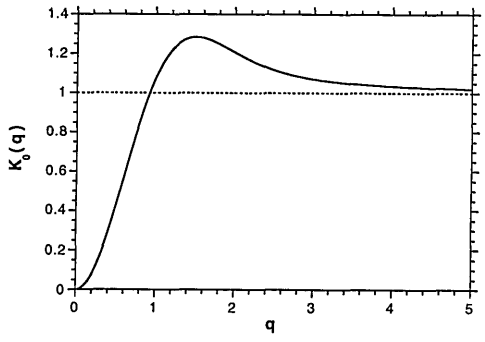

Fig. 5. Function K_0 given by Eq. (41), where $q = Wf_x = \theta/\theta_0$.

In the case of fractal surfaces the spectrum diverges at low frequencies and the vanishing of the kernel at that point plays an essential role. Even so, the spectral integral can still be viewed as a mean-square roughness value, but one that is no longer an intrinsic property of the surface since it depends on the system coherence length W.

The surface and system effects can be separated, however, and Eq. (40) can be written in terms of intrinsic finish parameters by expressing K_0 in terms of powers of $(Wf_x)^2$ and examining individual terms. For example, if we approximate it as

$$K_0(f_x') \approx \begin{cases} 2(Wf_x')^2 & 0 \leq f_x' \leq 1/\sqrt{2}W \\ 1 & \text{otherwise} \end{cases}, \qquad (42)$$

we obtain the following neat result for the reduction of the on-axis intensity:

$$\frac{I(0)}{I_s(0)} \approx 1 - \frac{4}{\theta_0^2}(\mu_0^2 + \mu_W^2) - \left(\frac{4\pi}{\lambda}\right)^2 \sigma_W^2, \qquad (43)$$

where μ_0 is the rms figure gradient, which is related to its profile spectrum according to Eq. (20), and

$$\mu_W^2 = 2\int_0^{1/\sqrt{2W}} df_x' S_1(f_x')(2\pi f_x')^2, \qquad (44)$$

$$\sigma_W^2 = \int_{1/\sqrt{2W}}^\infty df_x' S_1(f_x') \qquad (45)$$

are the band-width-limited values of the rms gradient and height of the finish errors.[13] Note that these quantities are finite for fractal surfaces, although their intrinsic values, determined by letting the limits go from zero to infinity, are undefined (infinite).

This approximate expression for the on-axis Strehl ratio has simple and interesting dependencies on system parameters. The factor of $1/\theta_0^2$ multiplying the surface-gradient terms comes from the curvature of the system spread function on the optic axis and is independent of λ in the case of system-limited optics, which means that these terms affect the image according to the rules of geometrical optics. The coefficient of the surface-roughness term, on the other hand, depends on the radiation wavelength but is indepen-

dent of the system spread function, which accounts for its historical precedence in the literature.

In other words, Eqs. (43)–(45) show that in the smooth-surface limit, spatial wavelengths of the profile errors that diffract within the $\exp(-1/2) = 0.607$ intensity point of the system spread function affect the on-axis intensity according to the rules of geometrical optics, while those that diffract outside that point deplete the core intensity without changing its shape.

B. Effects on the Image Width

The quadratic term in the expansion of the image intensity about the optic axis determines the effects of the surface errors on the image width. There are a number of ways to define image widths, the most obvious being the rms width. This measure, however, diverges when the image involves scattering from objects with infinite rms slopes, such as unapodized apertures, surfaces with exponential correlation functions, and fractal surfaces. In such cases the simplest practical measure is the parabolic width, that is, the half-width of the base of a parabola fitted to the apex of the image intensity:

$$\text{width } I(\theta) \triangleq \left[-\frac{1}{2}\frac{d^2}{d\theta^2}\left\{\frac{I(\theta)}{I(0)}\right\}_0 \right]^{-1/2}. \tag{46}$$

The parabolic and rms widths of a two-dimensional Gaussian are the same, namely, θ_0.

The effect of errors on the parabolic image width is given by

$$\frac{\text{width } I(\theta)}{\text{width } I_s(\theta)} = 1 + \left(\frac{4\pi}{\lambda}\right)^2 \int_0^\infty df_x' S_1(f_x') K_2(f_x'), \tag{47}$$

where the kernel

$$K_2(f_x') = 2(Wf_x')^2 {}_1F_1[2; 3/2; -(Wf_x')^2] \tag{48}$$

determines how the different frequency components in the surface profile affect the image width, just as K_0 discussed above determines their effects on the Strehl ratio.

This new factor is shown in Fig. 6. It shows that very long and very short spatial wavelengths have little effect on the image width, while those with wavelengths of the order of the coherence length W have maximum effect. This is reasonable since those are the wavelengths that diffract to the steepest part of the system spread function where a little does a lot.

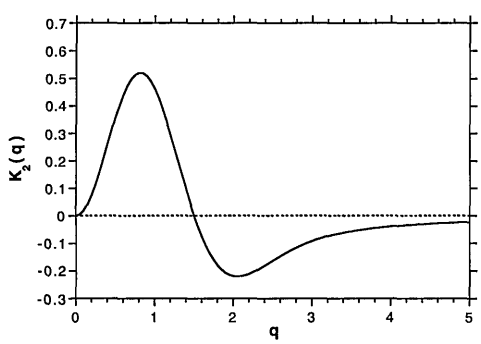

Fig. 6. Function K_2 given by Eq. (48), where $q = Wf_x = \theta/\theta_0$.

Equation (47) is also valid for any form of the surface spectrum. The width correction for conventional surfaces is essentially negligible but is significant for fractal surfaces because of their strong low-frequency components.

Equation (47) can be viewed as a Strehl-type correction with a different form of the effective surface roughness, or alternatively, in terms of an effective surface gradient by taking the factor of W^2 in Eq. (48) outside the integral and by using Eq. (20).

To separate surface and system effects, we try to approximate K_2 in terms of low powers of $(Wf_x)^2$, although this is more difficult than in the case of K_0. But if we concentrate on the low-frequency region, which is important for fractal surfaces, we can make the Procrustian approximation

$$K_2(f_x') \approx \begin{cases} 2(Wf_x')^2 & 0 \leqslant f_x' \leqslant 1/\sqrt{2}W \\ 0 & \text{otherwise} \end{cases}. \tag{49}$$

This means that the parabolic image width is broadened by the factor

$$\frac{\text{width } I(\theta)}{\text{width } I_s(\theta)} \approx 1 + \frac{2}{\theta_0{}^2}(\mu_0{}^2 + \mu_W{}^2), \tag{50}$$

where μ_0 is again given by Eq. (44).

It is interesting that this result depends only on slope or gradient errors of the surface but not its roughness; that is, it is a purely geometric-optics effect. Also, the factor $1/\theta_0{}^2$ appearing in Eq. (50) now arises from both the second and fourth derivatives of the system spread function along the optic axis.

9. System Performance and Surface Specification

A. Image Intensity and Width

Equations (43) and (50) show the effects on the image intensity and width in terms of bandwidth-limited values of the rms surface gradient and roughness.

Consider our example above of 140-Å radiation and a 100-μrad source–detector width [Eq. (14)]. If we require that each of the three error terms in Eq. (43) be $<10\%$, we find that μ_0 and μ_W must be <15.8 μrad, i.e., the rms slopes of the figure and finish profiles must each be <11.2 μrad, and the rms finish roughness must be <3.53 Å.

Similarly, a requirement that each of the two error terms in Eq. (50) be $<10\%$ leads to requirements on the gradient and slope terms that are less restrictive than those derived from the on-axis Strehl factor by a factor of 1.41.

These slope and roughness requirements are strict but appear to be within present manufacturing capabilities.[14]

B. Intensity of the Image Tail

Equation (38) shows that in the smooth-surface limit a requirement on the intensity well away from the image core translates to a requirement on the two-dimensional finish spectrum. This in turn is related to specific finish parameters through the form of the finish spectrum involved; Eqs. (22) and (36) show an example for conventional surfaces, and Eqs. (25) and (39) show general results for fractal surfaces.

C. Image-Frequency Distribution

The performance requirements considered above are given in terms of the image-intensity distribution in the focal plane. Perhaps the simplest requirements on the image are stated in terms of its spatial-frequency content in that plane, which is nothing more than the total OTF expressed in terms of that new frequency **g**:

$$\mathrm{OTF}(\mathbf{g}) = \mathrm{OTF}_s(\mathbf{g}) \times \exp\left[-\frac{1}{2}\left(\frac{4\pi}{\lambda}\right)^2 D(\mathbf{g})\right], \quad (51)$$

where $\mathbf{g} = \mathbf{f}/\lambda F$. One specification might be that the total OTF must be greater than, say, 0.8 at a particular frequency.

D. Hopkins Ratio

A more general condition is to require that the Hopkins ratio,

$$H(\mathbf{g}) = \frac{\mathrm{OTF}(\mathbf{g})}{\mathrm{OTF}_s(\mathbf{g})}, \quad (52)$$

be greater than some function or value.[15] Since Eqs. (51) and (52) involve the exponential dependence on the structure function, they are not limited to the smooth-surface approximation.

In general, performance requirements on the image intensity lead to conditions on the spectrum of the errors, while those on the OTF place conditions on its structure function.

10. Physical Interpretation

Both the parametric and nonparametric expressions for the image-intensity distribution are finite for fractal surface, even though the fractal spectrum diverges at long spatial wavelengths, which suggests that the scattering should diverge at small angles.

Physically, the divergence disappears since the finite size of the imaging optic makes the system insensitive to surface wavelengths longer than its diameter D_0, and the wavelengths between D_0 and W are attenuated by convolution with the nonvanishing source and detector sizes.

There is an interesting corollary to this. Most calculations of surface scattering are based on the model of an infinite surface coherently illuminated by an incident plane wave, i.e., $W = \infty$ in our notation.[16–19] In that case the only way to avoid small-angle divergences is to require that the error spectrum be well behaved at low frequencies, which means that the surface roughness itself must involve a finite-length scale or correlation length. In other words, pure plane-wave scattering calculations require conventional surfaces.[12]

In the present paper we point out that in real-world situations the finish of high-performance surfaces are frequently fractal and that in those cases the finite outer length scale required for finite scattering is introduced by system parameters, either the finite size of the optic for diffraction-limited optics or the system coherence length W for system-limited optics.

Finally, it is interesting to note that the fractal finish may be expected since the essence of a well-finished surface is that it is featureless, or in mathematical terms, that it is self-affine or fractal.

11. Summary

We have described a simple diffraction calculation for predicting the image of an imperfect mirror in terms of system and surface properties. When the imaging is system limited, as is frequently the case for x-ray optics, the diffraction integral depends on the effective coherence length of the radiation on the mirror surface, which is smaller than its aperture, as well as the error properties of the surface.

Roughly speaking, those spatial-wavelength components of the mirror-shape errors that are longer than the coherence length behave according to the rules of geometrical optics, while those with shorter spatial wavelengths behave according to diffraction optics.

In the smooth-surface limit, parametric and nonparametric expressions are given that can be used to specify surface properties in terms of performance requirements. The parametric expressions are functions of parameters of specific finish models, while the nonparametric forms are expressed in terms of the profile-power spectral density of the surfaces which can be measured directly in the laboratory.

Results are illustrated for two models: figure plus conventional finish, where the finish correlation length is comparable with or smaller than the coherence length, and figure plus fractal finish, where the correlation length is larger than the coherence length or effectively infinite. The results are well behaved even in the limiting case of pure fractal surfaces, where the correlation length becomes infinite and the power spectral density diverges at low frequencies.

References and Notes

1. E. L. Church and P. Z. Takacs, "Prediction of mirror performance from laboratory measurements," in *X-Ray/EUV Optics for Astronomy and Microscopy*, R. B. Hoover, ed., Proc. Soc. Photo-Opt. Instrum. Eng. **1160,** 323–336 (1989). This reference discusses the system-limited behavior of glancing-incidence mirrors in terms of their one-dimensional or profile power spectra.
2. E. L. Church and P. Z. Takacs, "Specification of the surface figure and finish of optical elements in terms of system performance," in *Specification and Measurement of Optical Systems*, L. R. Baker, ed., Proc. Soc. Photo-Opt. Instrum. Eng. **1781,** 118–130 (1992). This reference extends the research in Ref. 1 to normal-incidence optics and expresses the results in terms of the two-dimensional or area power spectra.

3. E. L. Church and P. Z. Takacs, "Specifying the surface finish of x-ray mirrors," in *Soft-X-Ray Projection Lithography,* Vol. 18 of OSA Proceedings Series (Optical Society of America, Washington, D.C., 1993). This reference extends the research in Ref. 2 to diffraction-limited optics.
4. The Gaussian forms of Eq. (15), (31), (32), and (51) follow from the assumption that the error fluctuations are members of a Gaussian random process with a Gaussian height distribution. In the more general case of a kth-order gamma distribution, Eq. (15) is replaced by $\mathrm{OTF}(\tau) = [1 + (4\pi/\lambda)^2 D(\tau)/2k]^{-k}$. In the smooth-surface limit, however, results are independent of the form of the height distribution.
5. The statistical stability of the results is ensured by the smallness of the parameter $(W/D_0)^2$.
6. $S_1(f_x)$ and $S_2(f)$ are the cosine and zeroth-order Hankel transforms of a common correlation function and form, then, an Abel-transform pair. That is, S_1 is the two-to-one-dimensional stereological projection or half-integral of S_2. See also Ref. 9.
7. E. L. Church and P. Z. Takacs, "Instrumental effects in surface finish measurements," in *Surface Measurement and Characterization,* J. M. Bennett, ed., Proc. Soc. Photo-Opt. Instrum. Eng. **1009,** 46–55 (1988).
8. E. L. Church and P. Z. Takacs, "The optimal estimation of finish parameters," in *Optical Scatter: Applications, Measurement, and Theory,* J. C. Stover, ed., Proc. Soc. Photo-Opt. Instrum. Eng. **1530,** 71–86 (1991).
9. E. L. Church, H. A. Jenkinson, and J. M. Zavada, "Relationship between surface scattering and microtopographic features," Opt. Eng. **18,** 125–136 (1979).
10. E. L. Church, "Fractal surface finish," Appl. Opt. **27,** 1518–1526 (1988). The coefficient 45 in Eq. (A5) of this reference should read 74.
11. The bars over the two-dimensional power spectra in Eqs. (33) and (38) denote their convolution with the system spread function, Eq. (13). This has a negligible effect for polished surfaces but would, for example, determine the nonvanishing widths of the spectral lines caused by periodic tool marks in machined surfaces.
12. Statistical scattering theory depends on the structure function of the surface-height fluctuations and not their autocovariance function. The structure function exists when the fluctuations have statistically stationary first differences, while the autocovariance function exists only in the more restrictive condition that the magnitudes themselves are also stationary. Fractal surfaces have stationary differences but nonstationary magnitudes, while conventional surfaces have stationary differences *and* magnitudes. A telltale difference is whether the surface in question has a finite intrinsic rms roughness. Conventional surfaces do; fractal surfaces do not.
13. More precisely, the limits 0 and ∞ in Eqs. (44) and (45) are $2/D_0$ and $2/\lambda$.
14. Melles Griot Industrie (France) advertises x-ray mirrors with rms slopes of < 5 μrad and rms roughnesses of < 5 Å. An rms slope of 5 μrad corresponds to an rms gradient of 7 μrad.
15. H. H. Hopkins, "The aberration permissible in optical systems," Proc. Phys. Soc. London Sec. B **52,** 449–470 (1957).
16. P. Beckmann and A. Spizzichino, *The Scattering of Electromagentci Waves from Rough Surfaces* (Pergamon, New York, 1963).
17. S. K. Sinha, E. B. Sirota, S. Garoff, and H. B. Stanley, "X-ray and neutron scattering from rough surfaces," Phys. Rev. B **38,** 2297–2311 (1988).
18. D. G. Stearns, "X-ray scattering from nonideal multilayer structures," J. Appl. Phys. **65,** 491–506 (1989).
19. D. G. Stearns, "X-ray scattering from interfacial roughness in multilayer structures," J. Appl. Phys. **71,** 4286–4298 (1992).